Catalytic hydrogenation of furfural to tetrahydrofurfuryl alcohol using competitive nickel catalysts supported on mesoporous clays

C. Sunyol[a]; R. English Owen[a], M. D. González[a], P. Salagre[a], Y. Cesteros[a*]

[a]Universitat Rovira i Virgili, Departament de Química Física i Inorgànica, C/ Marcel·lí Domingo 1, 43007 Tarragona, Spain

Prof. Yolanda Cesteros

Dpt. Química Física i Inorgànica

Universitat Rovira i Virgili

C/Marcel·lí Domingo 1

43007 TARRAGONA, Spain

Tel: +34 977558785

Fax: +34 977559563

e-mail: yolanda.cesteros@urv.cat

*To whom correspondence should be addressed.

Abstract

Nickel catalysts supported on mesoporous clays with different acid properties, such as montmorillonite MK-10, Al-pillared montmorillonite, mesoporous Na-saponite and mesoporous H-saponite, were prepared, characterized and tested for the hydrogenation of furfural to tetrahydrofurfuryl alcohol (THFA). Clays were also modified introducing basicity through magnesium oxide in different amounts. Catalysts with higher acidity or low amounts of metallic centres favoured deactivation and/or selectivity to the non-desired products. Interestingly, the addition of MgO both neutralized the acidity of the montmorillonite supports and improved the hydrogenation of the furanic ring, resulting in higher selectivity to THFA. The best catalyst was the one prepared with montmorillonite MK-10 covered by 30 wt% of magnesium oxide and with 8.8 % of the Ni metal phase achieving total conversion and total selectivity to THFA. The activity of this catalyst was maintained after several reuses.

Keywords: mesoporous clays; nickel catalysts; THFA; hydrogenation of furfural; acidity; MgO; mesoporous clays.

1. Introduction

Production of chemical compounds and fuels from biomass sources is acquiring importance as a more environmentally friendly alternative to non-renewable crude oil. Lignocellulose, one of the most abundant and low-price biomass feedstocks, mainly consists of three types of polymers: cellulose, hemicellulose, and lignin. Catalytic dehydration of xylose, extracted from hemicellulose, led to the formation of furfural, an interesting platform molecule, which can be later converted into high-added value products [1]. Thus, catalytic hydrogenation of furfural results in the formation of different products of interest, such as furfuryl alcohol (FOL), cyclopentanone (CPO) or tetrahydrofurfuryl alcohol (THFA), among others [2]. Of all of them, THFA is the most important hydrogenated product because of its use as environmental friendly solvent [2].

Classical synthesis of tetrahydrofurfuryl alcohol involves two steps, with the formation of furfuryl alcohol as intermediate. The reaction can be carried out in liquid or gas phase [3]. However, side reactions can also occur, including rearrangements, resulting mainly in the formation of cyclopentanone and cyclopentanol (CPL) in slightly acid aqueous conditions [4] (Scheme 1).

Good results were achieved using noble metals for the direct hydrogenation of furfural to THFA, especially with Pd, Rh and Ru [5-7], but their high cost make researchers look for cheaper alternatives, mainly catalysts based on Ni [7] or Cu [8]. Nickel supported on carbon nanotubes catalyst led to 84.3 % yield to THFA at 130 ºC and 40 bars of H_2 pressure after 10 h of reaction [9], a Ni/C catalyst derived from MOFs resulted in total conversion and total selectivity to THFA at 120 ºC and 10 bars of H_2 pressure after 2 h of reaction [10], and a Ni/γ-Al_2O_3 catalyst gave conversion up to 99.8

% and selectivity to THA of 99.5 % at 80 ºC and 40 bars of H_2 pressure after 2 h of reaction [11]. More recently, bimetallic MOF derived Ni-Co alloy catalyst presented almost total conversion and 99.1 % THFA selectivity at 80 ºC, 30 bars of H_2 pressure and 8 h of reaction [12], and Ni-Cu catalyst supported on mesoporous hectorite prepared with Ni:Cu ratio of 1:1 showed total conversion and selectivity to THFA of 95 % at 140 ºC and 40 bar H_2 pressure after 4 h of reaction [13].

Different catalytic systems were studied modifying the reaction conditions by applying higher H_2 pressure or much lower reaction temperatures. Nickel-cobalt catalysts supported on SBA-15 achieved 100 % of conversion and 90.4% of selectivity to THFA at 210 ºC, 70 bars of H_2 pressure and 6 h of reaction [14]. Ruan et al. reported high selectivity to furfuryl alcohol (FOL) (90.0% at 5 ºC and 92.4% at 10 ºC) at 50 bars of H_2 pressure and 1 h of reaction using a Pd/Ni/$Ni(OH)_2$/C catalyst [15]. Nakagawa et al. obtained 94 % of selectivity to THFA using a Pd–Ir/SiO_2 bimetallic catalyst at very low temperature (2 ºC) after 6 h of reaction but 80 bar of hydrogen pressure was required [16].

The presence of Brønsted and Lewis acidity can result in the production of humines, an undesired by-product, which can affect the activity of the metallic phase. Y. Yang et al. modified the support with basic oxides of alkaline metals (Mg, Ca, Sr, or Ba) [3]. Thus, changing the basic conditions with a Ni/Ba-Al_2O_3 catalyst they achieved >99% of furfural conversion and 99% of THFA selectivity. Therefore, finding a support with appropriate acid–base properties and porosity (to improve the metal phase dispersion and reducibility) becomes a challenge since it has not been practically studied.

Clay minerals are widespread materials on Earth. Saponite, $M_{x-y/n}[(Mg_{6-y}Al_y)^{Td}[(Si_{8-x}Al_x)^{Oh}.O_{20}(OH)_4].nH_2O$, is a trioctahedral microporous clay of the smectite group

containing an octahedral (Oh) sheet of MgO between tetrahedral (Td) sheets of SiO_2. Isomorphous substitution of Si^{4+} by Al^{3+} generates a negative layer charge, which should be compensated by the presence of interlayer cations (M^{n+}). Mesoporous saponites can be synthesized by adding quaternary ammonium salts or polymers during the hydrothermal treatment, and later removing of the template by calcination resulting in high-surface area materials [17-18].

In this work, several nickel supported on mesoporous clays catalysts, with different acid properties, were tested for the hydrogenation of furfural to obtain tetrahydrofurfuryl alcohol in liquid phase. Commercial acid montmorillonite clays (MK-10 and Al-Pillared) and synthesized Na-, H-saponites, directly and modified with different amounts of MgO, were used as supports since they have acidity that can be easily modified, high surface areas, mesoporosity and are of low cost. Special attention will be paid to the study the effect of adding MgO to the supports on the acidity of the final catalysts, and therefore, on the catalytic reaction. The percentage of metal phase was also modified changing the percentage of metal precursors and applying different reduction temperatures. The amount of metallic centres, responsible for the obtention of THFA, could also contribute to partially cover the acid sites responsible for undesired products. All catalysts were widely characterized.

2. Experimental

2.1.Reagents and commercial materials

Furfural was distilled under reduced pressure before use. Tetrahydrofurfuryl alcohol, montmorillonite MK-10 (M), aluminium pillared montmorillonite (PM), nickel (II) nitrate hexahydrate, magnesium nitrate hexahydrate, aluminium (III) nitrate

nonahydrate, copper (II) chloride dihydrate, ammonium nitrate, sodium silicate solution, ethylenediamine, cyclohexylamine and 1-butanol were of analytic grade and purchased from Sigma-Aldrich. Sodium hydroxide and sodium bicarbonate were purchased from EBRA reagents. Dodecyltrimethylammonium chloride, furfuryl alcohol were supplied by Acros Organics. Cyclopentanol and cyclopentanone were purchased from Alfa Aesar.

2.2.Preparation of mesoporous saponites

Saponite with general formula $Na_{1.2}Si_{6.8}Al_{1.2}Mg_6O_{20}(OH)_4 \cdot nH_2O$ was prepared. The ratios of the elements were determined from the moles of each reagent used in the initial slurry. The general method used to prepare these materials was that proposed by Gebretsadik et al. [18] with several modifications. A buffer solution of CO_3^{2-}/HCO_3^- was prepared at pH 13 by dissolving 3.63 g of NaOH and 6.6 g of $NaHCO_3$ in 50 mL distilled water. 2.7 g of the surfactant, dodecyltrimethylammonium chloride was added and stirred mechanically until no lumps resided. After which 5.6 mL of sodium silicate solution ($SiO_2 \cdot NaOH$, SiO_2 27 wt%, density 1.39 g/mL) was then added and stirred for a further 10 minutes. A second solution of 2.31 g of $Al(NO_3)_3 \cdot 9H_2O$ with 7.91 g of $Mg(NO_3)_2 \cdot 6H_2O$ in 5 mL distilled water was prepared. This was added dropwise to the stirring mixture over a period of half an hour. The final slurry was then stirred for a further 30 minutes ensuring homogenised stirring. The gel was then transferred into a conventional reactor and aged at 180 ºC for 72 h. The resulting solid was then filtered and washed with doubly deionised water to neutrality and then dried overnight in an oven at 80 ˚C. The surfactant was removed by calcination in a quartz tubular reactor in a two-step process, in the first at 550 ºC under 2 mL/s flow of air for 12 h, and in the

second at 600 ºC under 2 mL/s flow of oxygen for 12 h (sample S). The delaminated saponite should have Na cation in the interlamellar space. A saponite with Brønsted acidity will be also prepared by exchange with a 1 M $NH_4(NO_3)$ solution by refluxing for 1 h, resulting in the support HS.

2.3. Basic-modification of synthesized and commercial mesoporous clays

Basic modification of the supports was made through impregnation. First, an ethanolic solution 100 mL $Mg(NO_3)_2$ 1 M was prepared to impregnate 1 g of the desired clay (M, PM and S) with 23 mL and 4.6 mL of the $Mg(NO_3)_2$ solution to prepare catalysts with 30 wt% and 10 wt%, respectively. Then, the solvent was removed using a rotary evaporator, dried at 80 ºC and calcined at 350 ºC for 5 h in order to obtain supported magnesium oxide. The modified supports were named as MgO(10)-M, MgO(30)-M, MgO(30)-PM and MgO(30)-S.

2.4. Preparation of catalysts

Catalysts were prepared by impregnation. Firstly, an ethanolic solution $Ni(NO_3)_2$ 0.5 M was prepared. Secondly, 6 and 25 mL of nickel (II) nitrate solution were added to 1 g of the support in order to achieve 15 wt% or 40 wt% of nickel, respectively. Then, the solvent was rotary-evaporated and the residing solid heated at 80 ºC overnight. The samples were calcined at 450 ºC for 5 h in order to obtain the catalytic precursors named as P-Ni(15)/M, P-Ni(40)/M, P-Ni(40)/PM, P-Ni(40)/S, P-Ni(40)/HS, P-Ni(40)/MgO(10)-M, P-Ni(40)/MgO(30)-M, P-Ni(40)/MgO(30)-PM and P-Ni(40)/MgO(30)-S. The reduction of the catalytic precursors was carried out in a fluidized bed tubular reactor at 1.25 mL/s of H_2 flow at 450 ºC for 6 h resulting in

catalysts Ni(15)/M, Ni(40)/M, Ni(40)/PM, Ni(40)/S, Ni(40)/HS, Ni(40)/MgO(10)-M, Ni(40)/MgO(30)-M, Ni(40)/MgO(30)-PM and Ni(40)/MgO(30)-S. One more catalyst, Ni(40)/M (LT), was obtained by reducing P-Ni(40)/M at 1.25 mL/s of H_2 flow at 350 ºC for 6 h.

2.3.Characterization techniques

X-Ray diffraction was used to determine the crystalline phases, estimate the NiO and Ni crystallite size using the Scherrer equation [19] and quantify crystalline phases. The experiments were carried out with a Siemens D-500 instrument by using CuKα radition with a Ni filter and detecting values 2θ between 0 and 70º. Crystallite size was determined by Rietveld refinement [20] and it was performed with the TOPAS v6 software [21-22]. The background was modelized with a 2nd order Chebyschev polynomial. The instrumental contribution to the diffraction profile was calculated with the Fundamental Parameters Approach [23]. The relative quantitative phase analysis was obtained by refining the Rietveld scale factor for each phase and applying the corresponding well-known equations [24]. The peak width of each phase was modelled with the Double-Voigt Approach [25] by considering only the Lorentzian contribution of the crystallite size effect and discarding any contribution of the microstrain to the peak width. The averaged integral breadth was obtained from the resulting fitted Voigt function to the whole diffractogram.

The cation-exchange capacity was determined following the Bergaya and Vayer method [26]. The samples were exchanged with a 1 M solution of $[Cu(en)_2]^{2+}$ complex, and the exchanged amount was calculated by spectroscopic UV-Visible absorption at λ=546 nm

using a calibration curve at different concentrations. All measurements were done with a Shimadzu spectrometer following the Beer-Lambert law.

The surface area of the samples was calculated by nitrogen physisorption in a Quadrasorb Surface Analyzer instrument. Water and other physically adsorbed species were removed by pre-degassing the samples at 85 ºC for 12 h. The BET surface area was calculated using the Brunauer-Emmett-Teller equation. The pore size distribution was obtained using the Barrett-Joyner-Halenda (BJH) model.

Thermogravimetric analysis (TGA) of adsorbed cyclohexylamine (CHA) was carried out using a Setaram Labsys TG to determine acidity of the materials following the method previously applied for clays, zeolites and mesoporous materials [27-29],. This method involves thermogravimetric analysis following adsorption of the base on the catalysts and determines the number of acid sites, which are accesible and sufficiently strong to interact with the base after heat treatment at 250º C. Firstly, the samples were left in a solution of cyclohexylamine at room temperature overnight. Then, the samples were heated at 80 ºC for 4 h in order to eliminate excess of cyclohexylamine and for a further 2 h at 250 ºC to remove the physisorbed CHA. Finally, the samples were analysed using the TGA from 50 ºC to 800 ºC at 10 ºC/min under N_2. Acidity values were calculated from the weight loss observed between 250 ºC and 450 ºC.

Temperature Programmed Reduction (TPR) studies of the catalytic precursors were performed from room temperature until 900 ºC at 5 ºC/min under Ar/H_2 (95:5) in the same Setaram Labsys TG.

The morphologies and particle sizes of the samples were determined by transmission electron spectroscopy (TEM) on a JEOL JSM1011 electron microscopy operating at 80 kV.

2.4 Catalytic tests

Catalytic hydrogenation of furfural was performed in a 50 mL stainless steel autoclave equipped with a stirrer, a pressure valve and automatic temperature control apparatus. The reactor was connected to hydrogen flow. 30 g of aqueous solution was loaded into the reactor (1.5 g furfural) with 600 mg of catalyst. A small aliquot of this sample was kept aside for analysis by gas chromatography (GC). Then, the reactor was sealed and purged three times with H_2 for air removal. Afterwards, H_2 was fully charged into the reactor until 40 bar pressure, temperature programmed to 140 ºC and 600 rpm. The reaction lasted 4 h. The resulting solution was then left to cool and centrifuged in order to separate the reaction products from the catalyst. Afterwards, the filtrate was analysed by GC with an internal standard.

In order to study the reusability, the catalyst Ni(40)/MgO(30)-M was washed several times with ethanol and centrifuged to recover the catalyst and reused thrice at the same reaction conditions.

2.5. Analysis of the reaction products

GC measurements were performed on Shimadzu GC-2010A series equipped with an AOC-20i Series autoinjector and FID. The column was a Suprawax-280 (60 m x 0.25 µm x 0.50 µm). 1-Butanol was the internal standard. The quantification of products was determined based on GC data using internal standard method, which allowed for the determination of conversion and selectivity of the main products calculated as below.

$$Conversion\ (\%) = \frac{Concentration\ of\ converted\ furfural}{Concentration\ of\ initial\ furfural} x100$$

$$Selectivity\ (\%) = \frac{Concentration\ of\ furfural\ converted\ to\ the\ product}{Concentration\ of\ converted\ furfural} \text{x } 100$$

3. Results and Discussion

3.1. Characterization of supports

The four supports used in this study were materials related to smectite-type clays: two commercial mesoporous montmorillonites (M, PM) and two synthesized mesoporous saponites (S and HS). XRD pattern of the commercial montmorillonite MK-10 (M) allowed us to identify the presence of crystalline quartz and muscovite together with kaolinite and montmorillonite clay with disordered stacking of the layers. This mixture of components is because of the mineral nature of this sample. For commercial pillared clay (PM), in addition to the peaks corresponding to montmorillonite, two reflections 001, related to non-homogeneous pillars distribution, were also observed at low angles. Finally, synthesized mesoporous saponite samples (S and HS) showed the characteristic reflections corresponding to the saponite clay. The low definition of the 001 reflection in both samples can be related to disorder in the lamellae stacking as a result of delamination [18]. The common characteristics of these materials were their lamellar structure and mesoporosity, which was confirmed by TEM (not shown here). The textural and acid properties of the fourth supports are shown in Table 1.

Physisorption analysis of commercial montmorillonite MK10 (M) showed the capillary effect in the adsorption-desorption curve at high relative pressures (Isotherm type IV), typical of mesoporous materials, with a surface area of 220 m^2/g and an unimodal

porous size distribution with a radius around 18 Å. The isotherm of the aluminium pillared montmorillonite (PM) and its BET area (250 m^2/g) were similar to those corresponding to M (Table 1) but the pore size distribution was in this case bimodal, with an approximate pore radius of 20 and 30 Å, respectively. The area values obtained for both samples can be explained because the disorder in the lamellar structure for M, due to acid pre-treatment of the original mineral, and the presence of pillars for PM. In the case of the synthesized mesoporous saponites, an isotherm type IV was also observed for both samples, with an average pore size radius of around 20 Å and higher BET area (447-448 m^2/g), as expected, due to the delamination of small lamella [17-18]. Acidity information was obtained by thermogravimetric analysis of adsorbed cyclohexylamine (CHA-TGA). Due to its strong basicity, cyclohexylamine interacts with acid sites of varying strength including those that are weak. In order to exclude the weakest acid sites and therefore determine only those sites responsible for catalysis the samples were heat-treated at 250ºC [27]. Figure 1 shows three representative thermograms of the supports M, PM and HS. The mass loss percentage (blue line) was used to determine the mEq CHA/g while the temperature of the minimum of the first derivative (orange line) can be related to the acidity strength. The general tendency observed in these thermograms was the following: first, an initial mass loss, corresponding to the loss of water; and secondly, a loss in the range of 250-450 ºC associated to the desorption of CHA, related to the amount of acid sites [27-29]. The results showed an acidity for the M support of 0.42 mEq CHA/g and a temperature of the minimum of the first derivative at 347 ºC while for PM the acidity was 0.6 mEq CHA/g with a temperature of the minimum of the first derivative at 349 ºC (Table 1). For mesoporous saponites, the acidity was 0.7 and 1.2 mEq CHA/g for S and HS,

respectively, with a temperature of the minimum of the first derivative at 323 ºC and 357 ºC, respectively (Table 1). Moreover, outside of the range corresponding to the CHA desorption, a wide and less intense peak in the thermogram of the three samples was observed. This could be mainly associated with structural dehydroxylation [30]

Thus, we could evaluate the strength of acidity: the further to the left that the minimum of the first derivative, due to the acid site-CHA interactions, exists, the easier is to lose CHA and, in consequence, the weaker the acid sites. Therefore, HS presented the highest acidity and strength. In the case of S, mainly with Lewis acid sites, the acidity was higher than for M and PM, but CHA desorbed at a lower temperature (323 ºC). Besides, cation exchange capacity showed values of 0.56 for M, 0.17 for PM and 0.78 for S (Table 1). These results confirmed the higher capacity of S to exchange cations compared to M and PM. In fact, PM should have, probably, more protons that are more difficult to be exchanged, according to the measured value of acidity.

Regarding the supports modified with magnesium oxide, the isotherm was of type IV for MgO(10)-M but a significant decrease of the BET surface area, resulting in a value of 67 m^2/g, was observed when compared to M due to the partial coverage of the surface by MgO. This also reduced the initial pore radius of M. However, for MgO(30)-M, MgO(30)-PM and MgO(30)-HS, the isotherms were of type III, showing a N_2-surface interaction lower than that of adsorbate-adsorbate. Thus, a determination of the area was not possible for these samples. The acidity of the MgO-modified samples decreased as the amount of MgO on the clay was increased, as expected, caused by the neutralization of acid sites. Thus, the acidity value of M (0.42 mEq CHA/g) reduced to 0.21 mEq CHA/g for MgO(10)-M, and to 0 mEq CHA/g for MgO(30)-M.

3.2.Characterization of the catalytic precursors

X-ray diffraction patterns of the non-basic modified precursors confirmed the presence of nickel oxide for all of them. The NiO crystallite size values are shown in Table 2. An increase of the Ni content, from 15 to 40 wt%, increased the crystallinity of the NiO phase, as observed in Figure 2 when comparing P-Ni(15)/M (a) and P-Ni(40)/M (b). Thus, the characteristics peaks at 2Θ of 31.3º and 37.9º due to the NiO crystalline phase, were less intense and wider for P-Ni(15)/M, as confirmed by its lower NiO crystallite size (Table 2). By changing the support for the same Ni content (40 wt%), some differences in the crystallinity of NiO were observed. The NiO supported on mesoporous saponites, P-Ni(40)/S and P-Ni(40)/HS, presented smaller crystallite sizes (Table 2) than those supported on M or MP, probably due to the higher surface area of S and HS resulting in a greater dispersion. The smallest NiO crystallite size was observed for P-Ni(40)/HS (6.2 nm). This could be explained, in addition to its area, by the higher acidity of HS (Table 1), which can favor the dispersion of a basic oxide such as NiO.

Interestingly, for the NiO supported on MgO modified supports, the XRD patterns did not show separate peaks corresponding to MgO and NiO crystalline phases. In fact, the signal appeared between the two expected peaks. Considering that NiO has a space group $Fm\bar{3}m$, the same as MgO, and dimensions of a=b=c=4.1771 Å and 4.1980 Å, respectively, a solid solution may have formed. This hypothesis was based on the Vegard's law, an empirical rule that establishes a linear correlation, at constant temperature, between the cell parameters of the crystal of an alloy and the concentration of the constituent elements. Therefore, a solid solution type $Ni_xMg_{1-x}O$ was formed. This occurred in all the samples containing MgO. The greater the amount of MgO, the further the signal was shifted to lower angles (see Figure 2c). The crystallite size values

of the NiO-MgO solid solution phase were smaller than that of the NiO crystallites for the non-basic modified catalytic precursors (Table 2). The most significant decrease was observed when the support was PM, in which the size of the crystallite changed from 21.9 nm in P-Ni(40)/PM to 6.2 nm in P-Ni(40)/MgO(30)-PM. Therefore, in all cases the solid solution favoured dispersion.

Transmission electron microscopy showed, in detail, the supported particles of NiO, as darker zones, complementing the X-ray diffraction results. At 150k magnifications some NiO particles in P-Ni(15)/M were crystallized in the form of octahedrons with sizes around 10 nm in a good dispersion (Figure 3a). When the amount of NiO was increased (P-Ni(40)/M) the dispersion was not as good and the range of particle size was greater (10-80 nm) (Figure 3b). For the catalytic precursors containing magnesium oxide it was difficult to differentiate the particles because of the formation of the solid solution, showing a less intense colour of the NiO-MgO particles.

Nitrogen physisorption analysis of the catalytic precursors without basic modification showed a decrease of the BET area as the amount of NiO was increased (Table 2). The pore size, compared to the supports themselves, did not change significantly. This suggests that there was no priority occupation of pores. Precursors containing MgO, however, showed different values depending on the amount. In the samples containing 10 wt% of MgO, the decrease in area was associated with the occupation of the support surface with particles of solid solution MgO-NiO. Pore size distribution and average pore radius values exhibited some differences between samples. P-Ni(40)/M had a value of 17 Å while in P-Ni(40)/MgO(10)/M the pore distribution was bimodal, with average pore radius values of 19.5 and 40 Å, probably related to inter-particle space of particles with different size. On the other hand, when the sample contained 30 wt% of MgO (P-

Ni(40)/MgO(30)/M) the surface area increased and the bimodality disappeared leaving only a single pore size distribution of 20 Å. The conclusion was that the greater the amount of MgO, the greater the amount of solid solution and the better the dispersion of NiO. This resulted in the formation of smaller particles, in turn causing an increase in the surface area whilst the pore size distribution remained unimodal.

Acidity studies of the catalytic precursors were performed by TGA of adsorbed cychlohexylamine (CHA). The results are also shown in Table 2. The increase in the amount of NiO and MgO resulted in a decrease of acidity, as expected, to the extent that, for the catalytic precursors, which had a support modified with the 30 wt% of MgO and loaded with the highest amount of nickel, the acidity was completely neutralised (Table 2).

By comparing the TGA profiles of the samples P-Ni(15)/M, P-Ni(40)/M and P-Ni(40)/MgO(10)-M (Figure 4), a first derivative peak was observed around 347 ºC, at similar temperature to that of the support M itself (347 ºC, Figure 1). This means that neutralization was not preferential on stronger acid sites. At higher temperature (> 450 ºC), outside of the range corresponding to the CHA desorption, there was a narrow and intense peak in the thermogram of the three samples that could be mainly associated with dehydroxylation of hydrated NiO and/or the formation of CHA complexes with the nickel of NiO together with some structural dehydroxylation [30]. Finally, one more derivative peak was detected at 677 ºC in the catalytic precursors P-Ni(40)/M and P-Ni(40)/MgO(10)-M that was larger for the latter. This peak could be related to the formation of CHA complexes with interlamellar cations incorporated during impregnation with Ni or Mg. When the supports were PM, S and HS, acidity reduced as a result of the presence of NiO and MgO in the samples (Table 2), although the

derivative peak corresponding to CHA desorption showed similar temperatures to those observed for the corresponding support (Figure 5). The better dispersion of the NiO particles in these supports decreased the acidity amount of the saponites, meaning that the acid sites of the support were covered more efficiently. Additionally, the peak at 677 ºC, which was not observed for P-Ni(40)/HS, appeared for P-Ni(40)/S. This confirms that this peak should be related to the interaction between interlamellar Ni cations incorporated during impregnation and CHA since protonated saponite is more difficult to exchange than saponite.

In order to compare the NiO reducibility for the different catalytic precursors, temperature-programmed reduction studies were performed. The results are indicated in Table 2. The initial reduction temperature was similar for the precursors P-Ni(15)/M, P-Ni(40)/M and P-Ni(40)/PM with values around 338-345 ºC, but for the sample P-Ni(15)/M the rate of reduction was slower since the minimum corresponding to the first derivative appeared at higher temperature (480 ºC). In the group of the catalytic precursors supported on saponites, when the cation was Na (P-Ni(40)/S) the thermogram showed two mass losses in the range of determination (250-650 ºC) (Figure 6). Thus, it was apparent that there was a quantity of nickel that was more easily reduced (at 352 ºC) and a second quantity with lower reducibility (at 650 ºC). These peaks could be related to the different degrees of interaction between NiO and the saponite supports. A likely explanation is that the loss corresponding to the higher temperature could be due to Ni^{2+} introduced by exchange in the interlaminar space during impregnation of the support, resulting in a more difficult reduction. A similar phenomenon to this was observed in the case of saponites that were exchanged with a solution of nickel cations [31]. The catalytic precursors, whose supports were modified

with MgO, showed that the reduction started later and also finished later in all the cases. This can be explained by the presence of solid solution.

3.3.Characterization of the catalysts

Table 3 shows the XRD results obtained for all catalysts. The catalysts supported on M and PM, which were reduced at 450 ºC, had total reduction of nickel oxide, both for 15 wt% and 40 wt% of nickel content. The Ni crystallite size values were higher for the catalysts with the 40 wt% metal, as expected. When P-Ni(40)/M was reduced at 350 ºC (Ni(40)/M(LT)), the reduction was not complete (83%) and the Ni crystallite size was smaller. For the catalysts supported on saponites, which were reduced at 450 ºC, catalyst Ni(40)/HS showed a complete reduction while for catalyst Ni(40)/S the % of reduction was 55 %, in agreement with the lower reducibility of its precursor, as observed by TPR (Table 2). The Ni crystallite sizes of saponite supported nickel catalysts were smaller than those of the catalysts supported on commercial montmorillonite (Table 3).

Figure 7 shows the XRD patterns for the catalysts Ni(40)/MgO(10)-M, Ni(40)/MgO(30)-M and Figure 8 for the Ni(40)/MgO(30)-S. The presence of the NiO-MgO solid solution in all these catalysts, explains the lower reducibility of their NiO, as expected taking into account TPR results (Table 2). In the catalyst Ni(40)/MgO(30)-S (Figure 8) the % of Ni phase was very low (12%). In this case, both Ni^{2+} in the interlamellar space of saponite and the formation of the NiO-MgO solid solution made more difficult the NiO reduction.

4. Catalytic activity

With respect to the catalysts studied for this reaction, the effect of the two types of active sites present should be analysed: metal and acid sites. The metal sites are necessary for the reduction of the aldehyde functional group in furfural to furfuryl alcohol (the reaction intermediate) - a process that is easy to facilitate [5]. However, the second hydrogenation of the C=C linkage in the ring is more challenging [3] and the metal sites are in competition with the acid sites that catalyse the formation of secondary products, such as CPO, CPL and resinification products [32]. Therefore, the catalytic results depend on the relative amounts of the metal and acid sites and the relative activity of these sites. The results are shown based on the conversion of furfural and the selectivity to THFA, FOL, CPO and CPL that were calculated from the data obtained from gas chromatography. The rest of the products until 100 % should be resinification products, which cannot be detected by GC.

Figure 9 shows the catalytic activity results for the hydrogenation of furfural for all catalysts. Regarding the non-basic modified catalysts prepared with commercial supports and reduced at 450 ºC, high conversion (90-100 %) but low selectivity to THFA (13-25 %) values were obtained. Conversion values were slightly higher for those synthesized with montmorillonite MK-10 while the selectivity to THFA was slightly higher for that supported on PM. Higher amounts of CPO and CPL were formed with Ni(15)/M and Ni(40)/M whereas FOL was the main product for Ni(40)/PM. These small differences should be related to the relative activity of the acid and metal sites present in each catalyst. By comparing catalysts Ni(40)/M and Ni(40)/M (LT), the second one reduced at 350 ºC, conversion was total for both but the selectivity to THFA was lower for the catalyst reduced at lower temperature. This can be related to less amount of reduced Ni present in catalyst Ni(40)/M (LT) (Table 3). Furthermore, Ni

could not compete enough with the acid sites, so acid catalysis had higher contribution to catalysis than metal catalysis.

For catalysts using saponites as supports the conversion values were moderate (40-47 %) with similar low selectivity to THFA (around 15 %). Additionally, the selectivity to FOL was much higher than the selectivity to THFA for Ni(40)/S. An increase in the acidity of the support (Ni(40)/HS) resulted in a slight decrease of the conversion and the formation of higher amounts of CPO (Figure 9). These results confirm again the importance of the role of acid sites for this reaction, since this catalyst had 100 % of Ni phase (Table 3). The acidity probably promotes catalyst deactivation by the formation of resinification products that block the metal sites.

On the other hand, the introduction of basic sites in the M and PM supported catalysts, notably favoured the selectivity to tetrahydrofurfuryl alcohol. This could be explained by the lower/null amount of acid sites together with the lower amount of metallic sites present in these catalysts compared to their homologues Ni(40)/M and Ni(40)/PM (Tables 2 and 3). Thus, total selectivity and almost total selectivity to THFA was achieved for the catalysts with higher magnesium content, Ni(40)/MgO(30)-M and Ni(40)/MgO(30)-PM, respectively. Nevertheless, the presence of some acidity for the catalyst with the lowest MgO content, Ni(40)/MgO(10)-M, reduced the selectivity to THFA at expenses of increasing the formation of by-products like FOL and CPO although this catalyst had higher Ni content than Ni(40)/MgO(30)-M (Table 3). This confirms the importance of balancing acid and metal sites for this reaction. This supports again the idea that neutralisation of acid sites is essential for a successful selective reaction to THFA.

From our results and taking into account the results previously reported by Yang et al. [3], we believe that, in our catalysts, magnesium could coordinate with the oxygen from FOL, bringing it closer into the metallic surface and improving the hydrogenation of the furanic ring, to continue with the catalytic hydrogenation.

Conversely, the basic modified support in catalyst Ni(40)/MgO(30)-S yielded an increase of conversion (61%) but a decrease in the selectivity to THFA until 7 % at expenses of the formation mainly of high amounts of FOL. The low amount of metallic sites for this catalyst could explains these results.

The best catalyst, Ni(40)/MgO(30)-M, was chosen to study its reusability. Catalyst was reused thrice at the conditions commented in the experimental section. The results showed good stability of the catalyst (Figure 10). The loss of catalytic activity, including conversion and selectivity of THFA, was, on average, 5%. The test showed some increase in the production of FOL. This suggested the contamination by residual products on the surface of the catalyst that deactivated the catalyst especially after the first use. In order to evaluate the nature of the products remaining in the catalytic pores after reaction, the resulting solution obtained after washing and centrifugation of the reused catalyst was analyzed by gas chromatography. The chromatogram exhibited the presence of small peaks corresponding to furfural and some reaction products. However, XRD pattern of the reused catalyst did not show significant variations with respect to that taken for the fresh catalyst. An efficient wash of the catalyst was a crucial factor in obtaining good values of conversion and selectivity in later tests.

4. Conclusions

The hydrogenation of furfural is highly dependent on the amount of metallic nickel but also on the acidity of the catalysts. Higher values of acidity result in catalyst deactivation due to resinification products or higher selectivity to acid-catalysed products.

Catalysts containing MgO showed lower percentage of metallic nickel than their non-basic modified counterparts due to the formation of a NiO-MgO solid solution, which makes difficult the NiO reduction. For the catalyst supported on basic-modified saponite, in addition to the solid solution, the Ni^{2+} incorporated by exchange during impregnation in the interlamellar space was also very difficult to reduce. This resulted in the least amount of reduced nickel (12 %).

Catalytic results of non-basic modified catalysts showed high or moderate conversion but low selectivity values to the product of interest, THFA. The presence of acidity in these catalysts favoured the formation of byproducts, such as CPO, CPL or FOL. Interestingly, the addition of MgO neutralized the acidity of the clay support. This was essential for a successful reaction. As a result of that, total conversion and total selectivity to THFA was obtained with the catalyst Ni(40)/MgO(30)-M, which had the highest content of MgO and appropriate amounts of reduced nickel. This confirms the importance of balancing acid and metal sites for this reaction. After reusing thrice, this catalyst showed good stability with a loss of catalytic activity on an average of 5 %.

Acknowledgments

Authors acknowledge the finantial support of the Ministerio de Economía y Competitividad of Spain and Feder Funds (CTQ2015-70982-C3-3-R), and the recognition from the Generalitat de Catalunya (2017 SGR 798).

5. References

[1] C. M. Cai, T. Zhang, R. Kumar, C. E. Wyman, J. Chem. Technol. Biotechnol. 89 (2014) 2-10. https://doi.org/10.1002/jctb.4168

[2] Y. Nakagawa, H. Nakazawa, H. Watanabe, K. Tomishige, ChemCatChem 4 (2012) 1791-1797. https://doi.org/10.1002/cctc.201200218

[3] Y. Yang, J. Ma, X. Jia, Z. Du, Y. Duan, J. Xu, RSC Adv. 6 (2016) 51221-51228. https://doi.org/10.1039/C6RA05680F

[4] Y. Yang, Z. Du, Y. Huang, F. Lu, F. Wang, J. Gao, J. Xu, Green Chem. 15 (2013) 1932-1940. https://doi.org/10.1039/C3GC37133F

[5] Y. Nakagawa, K. Tomishige, Catal. Commun. 12 (2010) 154-156. https://doi.org/10.1016/j.catcom.2010.09.003

[6] B. M. Matsagar, C.-Y. Hsu, S. S. Chen, T. Ahamad, S. M. Alshehri, D. C. W. Tsang, K. C.-W. Wu, Sustainable Energy Fuels. 4 (2020) 293-301. https://doi.org/10.1039/C9SE00681H

[7] Y. Nakagawa, M. Tamura, K. Tomishige, ACS Catal. 3 (2013) 2655-2668. https://doi.org/10.1021/cs400616p

[8] J. Wu, G. Gao, J. Li, P. Sun, X. Long, F. Li, Appl. Catal. B: Environ. 203 (2017) 227-236. https://doi.org/10.1016/j.apcatb.2016.10.038

[9] L. Liu, H. Lou, M. Chen, Int. J. Hydrogen Energy 41 (2016) 14721-14731. https://doi.org/10.1016/j.ijhydene.2016.05.188

[10] Y. Su, C. Chen, X. Zhu, Y. Zhang, W. Gong, H. Zhang, H. Zhao, G. Wang, Dalton Trans. 46 (2017) 6358–6365. https://doi.org/10.1039/C7DT00628D

[11] S. Sang, Y. Wang, W. Zhu, G. Xiao, Res. Chem. Intermed.

43 (2017) 1179-1195. https://doi.org/10.1007/s11164-016-2691-8

[12] H. Wang, X. Li, X. Lan, T. Wang, ACS Catal. 8 (2018) 2121-2128. https://doi.org/10.1021/acscatal.7b03795

[13] V. Sánchez, P. Salagre, M. D. González, J. Llorca, Y. Cesteros, Mol. Catal. 490 (2020) 110956. https://doi.org/10.1016/j.mcat.2020.110956.

[14] J. Parikh, S. Srivastava, G. C. Jadeja, Ind. Eng. Chem. Res. 58 (2019) 16138–16152. https://doi.org/10.1021/acs.iecr.9b01443

[15] L. Ruan, H. Zhang, M. Zhou, L. Zhu, A. Pei, J. Wang, K. Yang, C. Zhang, S. Xiao, B. H. Chen, Mol. Catal. 480 (2020), 110639. https://doi.org/10.1016/j.mcat.2019.110639

[16] Y. Nakagawa, K. Takada, M. Tamura, K. Tomishige, ACS Catal. 4 (2014) 2718–2726. https://doi.org/10.1021/cs500620b.

[17] F.B. Gebretsadik, P. Salagre, Y. Cesteros, Appl. Clay Sci. 87 (2014) 170–178. https://doi.org/10.1016/j.clay.2013.10.027.

[18] F.B. Gebretsadik, D. Mance, M. Baldus, P. Salagre, Y. Cesteros, Appl. Clay Sci. 114 (2015) 20–30. https://doi.org/10.1016/j.clay.2015.05.004.

[19] A. R. Stokes, A. J. C. Wilson, Math. Proc. Cambridge Philos. Soc. 38 (1942) 313–322. https://doi.org/10.1017/S0305004100021988.

[20] H. M. Rietveld, J. Appl. Cryst. 2 (1969) 65–71. https://doi.org/10.1107/S0021889869006558.

[21] Bruker AXS GmbH, Software TOPAS 6, (2017).

[22] A. A. Coelho, J. Appl. Cryst. 51 (2018) 210-218. https://doi.org/10.1107/S1600576718000183.

[23] R. W. Cheary, A. A. Coelho, J. P. Cline, J. Res. Natl. Inst. Stand. Technol. 109

(2004) 1-25. https://doi.org/10.6028/jres.109.002.

[24] R. J. Hill, C. J. Howard, J. Appl. Cryst. 20 (1987) 467-474. https://doi.org/10.1107/S0021889887086199.

[25] D. Balzar, in: R.L. Snyder, J. Fiala, H.J. Bunge (Eds.), Defect and Microstructure Analysis by Diffraction (International Union of Crystallography Monographs on Crystal), Oxford University Press, Oxford, 1999, pp. 94-124.

[26] F. Bergaya, M. Vayer, Appl. Clay Sci. 12 (1997) 275-280. https://doi.org/10.1016/S0169-1317(97)00012-4.

[27] C. Breen, Clay Minerals 26 (1991) 487. https://doi.org/10.1180/claymin.1991.026.4.04

[28] R. Mokaya, W. Jones, S. Moreno, G. Poncelet, Catal. Lett. 49 (1997) 87-94. https://doi.org/10.1023/A:1019084617120.

[29] M. D. González, Y. Cesteros, P. Salagre, Appl. Catal. A: Gen. 450 (2013) 178-188. https://doi.org/10.1016/j.apcata.2012.10.028.

[30] M. Holtzer, A. Bobrowski, S. Zymankowska-Kumon, J. Mol. Struct. 1004 (2011) 102-108. https://doi.org/10.1016/j.molstruc.2011.07.040.

[31] I. Vicente, P. Salagre, Y. Cesteros, Appl. Clay Sci. 53 (2011) 212–219. https://doi.org/10.1016/j.clay.2010.12.025.

[32] S. Koso, N. Ueda, Y. Shinmi, K. Okumura, T. Kizuka, K. Tomishige, J. Catal. 267 (2009) 89-92. https://doi.org/10.1016/j.jcat.2009.07.010.

Table 1. Characterization of the supports.

Support	Surface BET area (m^2/g)	Average pore radius (BJH) (Å)	Acidity (mEq CHA/g) (TGA)*	Minimum 1st derivative of TGA (ºC)	C.E.C (mEq/g)
M	220	18	0.42	347	0.56
PM	250	20 and 30	0.60	349	0.17
S	448	20	0.70	323	0.78
HS	447	20	1.20	357	-

*calculated from cyclohexylamine desorbed between 250 and 450 ºC by TGA; C.E.C.: cation exchange capacity.

Table 2. Characterization of the catalytic precursors.

Catalytic Precursors	Surface BET area (m^2/g)	Average Pore radius (BJH) (Å)	Acidity (meq CHA/g) (TGA)	NiO crystallite size (nm) (XRD)	Initial Reduction temperature (ºC) (TPR)	Minimum of red. temp. (ºC) (TPR)
P-Ni(15)/M	186	17	0.32[a]	7.3 ± 0.2	343	480
P-Ni(40)/M	106	17	0.20 [a]	18.9 ± 0.3	338	437
P-Ni(40)/PM	93	20	0.23 [a]	21.9 ± 0.4	345	425
P-Ni(40)/S	384	20	0.13 [a]	7.5± 0.2	352; 650 (2 peaks)	525; 740
P-Ni(40)/HS	229	20	0.36 [a]	6.2± 0.1	401	492
P-Ni(40)/MgO(10)-M	28	19.5 and 40	0.17 [a]	12.2 ± 0.2 [b]	396	550
P-Ni(40)/MgO(30)-M	35	20	0	12.7 ± 0.2 [b]	340	600
P-Ni(40)/MgO(30)-PM	11	20	0	6.2 ± 0.2 [b]	366	729
P-Ni(40)/MgO(30)-S	115	20	0	6.8 ± 0.5 [b]	445	757

[a] calculated from cyclohexylamine desorbed between 250 and 450 ºC by TGA; [b] Crystallite size of the NiO-MgO solid solution.

Table 3. Characterization of the catalysts by XRD.

Catalysts	**% Ni (XRD)**	**% NiO (XRD)**	**% Solid Solution NiO-MgO (XRD)**	**Ni crystallite size (nm) (XRD)***
Ni(15)/M	100	0	0	6.8 ± 0.3
Ni(40)/M	100	0	0	22.2 ± 0.4
Ni(40)/M (LT)	83	17	0	19.7 ± 1.6
Ni(40)/PM	100	0	0	23.7 ± 0.4
Ni(40)/S	55	45	0	8.9± 0.2
Ni(40)/HS	100	0	0	7.9± 0.1
Ni(40)/MgO(10)-M	32	0	68	12.2 ± 0.2
Ni(40)/MgO(30)-M	22	0	78	12.7 ± 0.2
Ni(40)/MgO(30)-PM	21	0	79	6.2 ± 0.2
Ni(40)/MgO(30)-S	12	0	88	8.3± 0.5

*Crystallite size was determined by X-ray diffraction using the Scherrer equation.

LEGENDS AND CAPTIONS

Scheme 1. Products and by-products formed during hydrogenation of furfural.

Figure 1. CHA-TGA analyses of the samples: a) M, b) PM and c) HS. Blue line: thermogram. Orange line: first derivative. The temperature indicated on the figure corresponds to the minimum of the first derivative of the TGA between 250-450 ºC.

Figure 2. X-ray diffraction of the catalytic precursors: a) P-Ni(15)/M, b) P-Ni(40)/M. Purple Line: NiO phase, Green line: muscovite phase, Red line: quartz phase. c) Comparison of the XRD patterns for the catalytic precursors: Black line: P-Ni(40)/M; Red line: P-Ni(40)/MgO(10)-M; Blue line: P-Ni(40)/MgO(30)-M. Purple line: NiO phase.

Figure 3. TEM images of a) P-Ni(15)/M (150k) and b) P-Ni(40)/M (120 k)

Figure 4. CHA-TGA analyses of the catalytic precursors prepared with montmorillonite MK-10 as support: a) P-Ni(15)/M, b) P-Ni(40)/M and c) P-Ni(40)/MgO(10)-M Blue line: thermogram. Orange line: first derivative. The temperature indicated on the figure corresponds to the minimum of the first derivative of the TGA between 250-450 ºC.

Figure 5. CHA-TGA analyses of the catalytic precursors prepared with different supports: a) P-Ni(40)/PM, b) P-Ni(40)/S, and c) P-Ni(40)/HS. Blue line: thermogram. Orange line: first derivative. The temperature indicated on the figure corresponds to the minimum of the first derivative of the TGA between 250-450 ºC.

Figure 6. TPR of the catalytic precursor P-Ni(40)/S. Blue line: thermogram. Orange line: first derivative.

Figure 7. XRD pattern of the catalysts: a) Ni(40)/MgO(30)-M, and b) Ni(40)/MgO(10)-M. Blue line: Ni, Red line: NiO, Green line: MgO; * quartz; • muscovite.

Figure 8. XRD pattern of the catalyst Ni(40)/MgO(30)-S. Blue line: Ni, Red line: NiO, Green line: MgO; *: saponite.

Figure 9. Catalytic activity for the catalysts studied. Reaction conditions: 1.5 g of furfural, 140 ºC, 40 bar H_2, 4 h, 600 mg of catalyst.

Figure 10. Reutilisation tests for catalyst Ni(40)/MgO(30)-M. Reaction conditions: 1.5 g of furfural, 140 ºC, 40 bar H_2, 4 h, 600 mg of catalyst.

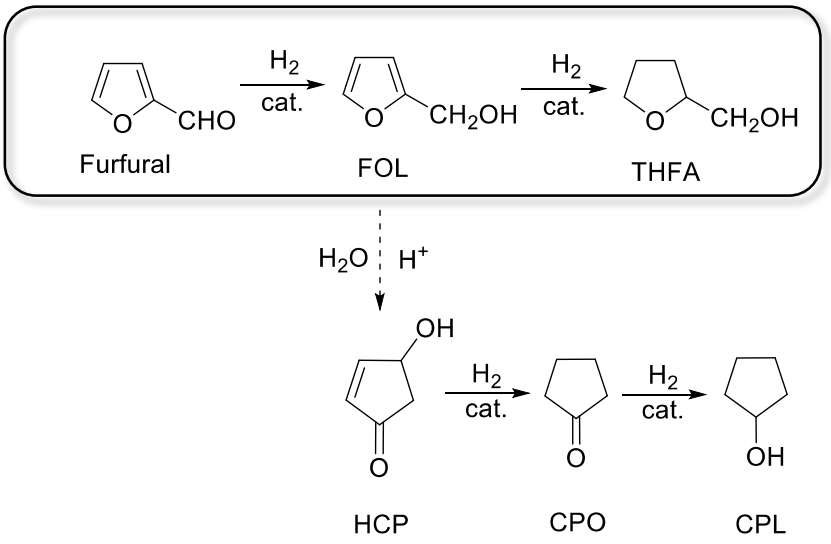
H2
cat.
H2
cat.
O
CHO
CH2OH
CH2OH
Furfural
FOL
THFA
H2O
H+
OH
H2
cat.
H2
cat.
O
O
OH
HCP
CPO
CPL

Scheme 1

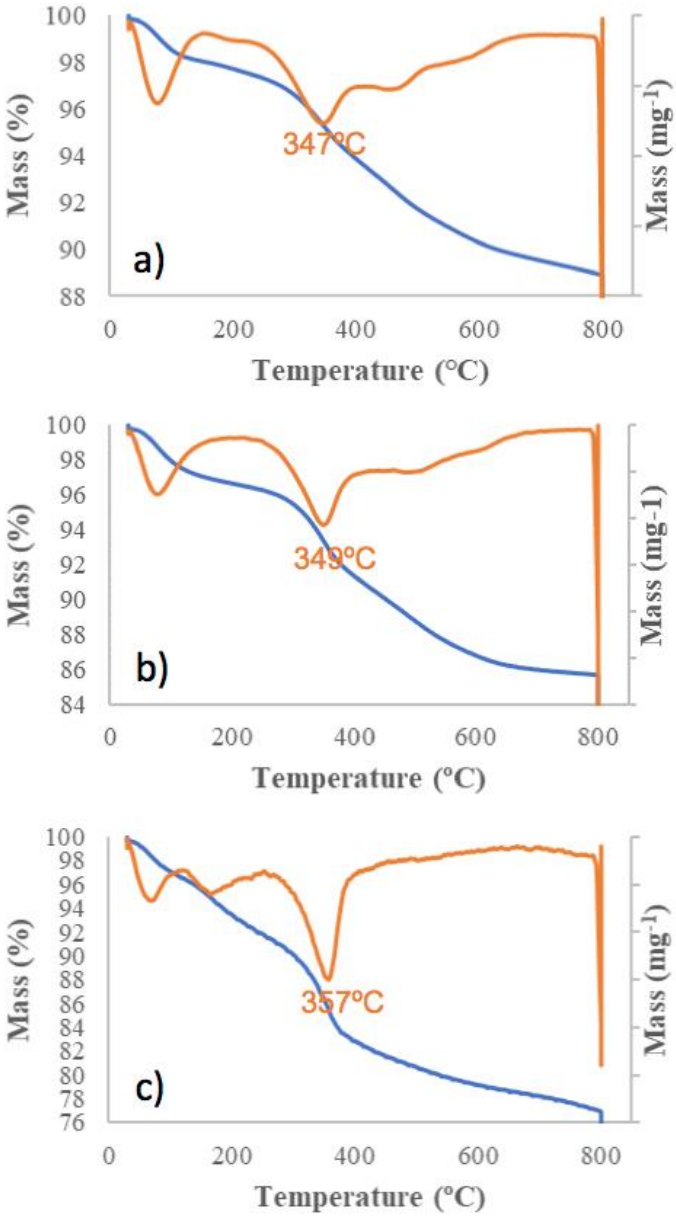
100
98
96
94
92
90
88
Mass (%)
347°C
a)
0
200
400
600
800
Temperature (°C)
Mass (mg-1)
100
98
96
94
92
90
88
86
84
Mass (%)
349°C
b)
0
200
400
600
800
Temperature (°C)
Mass (mg-1)
100
98
96
94
92
90
88
86
84
82
80
78
76
Mass (%)
357°C
c)
0
200
400
600
800
Temperature (°C)
Mass (mg-1)

Figure 1

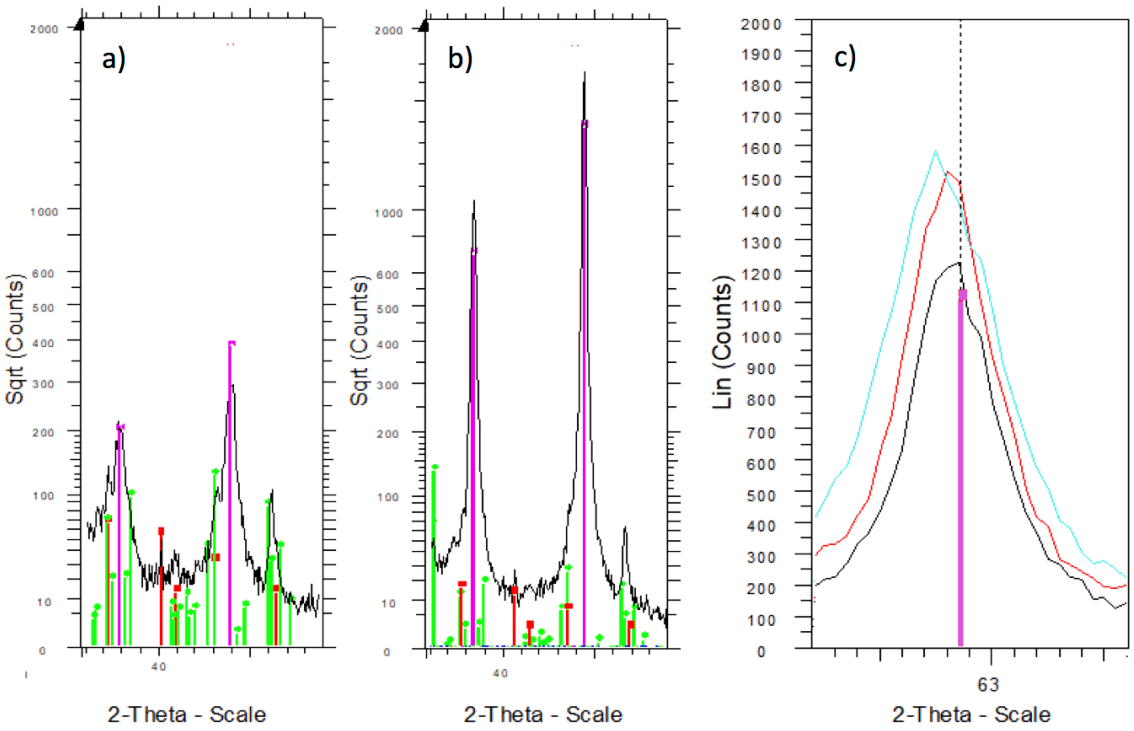
a)
b)
c)
Sqrt (Counts)
Lin (Counts)
2-Theta - Scale
2-Theta - Scale
2-Theta - Scale

Figure 2

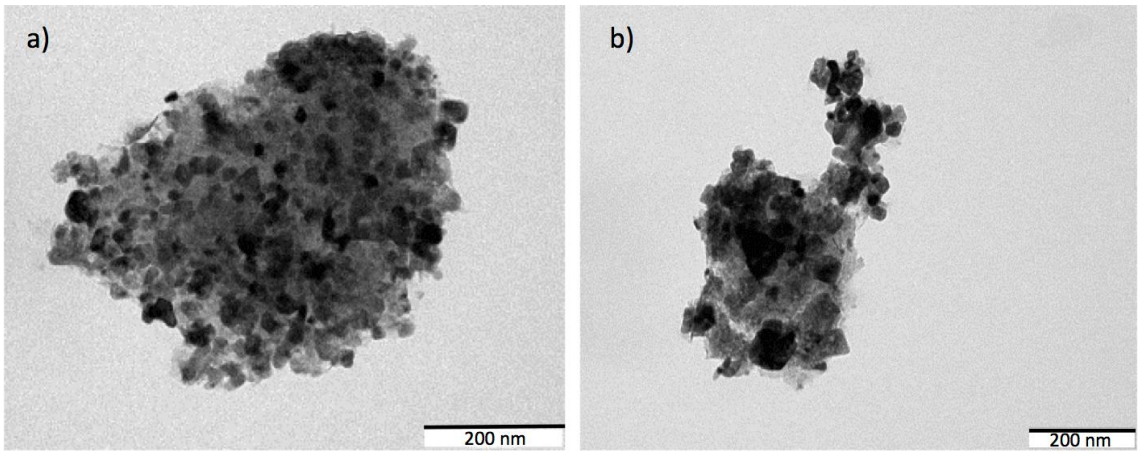

Figure 3

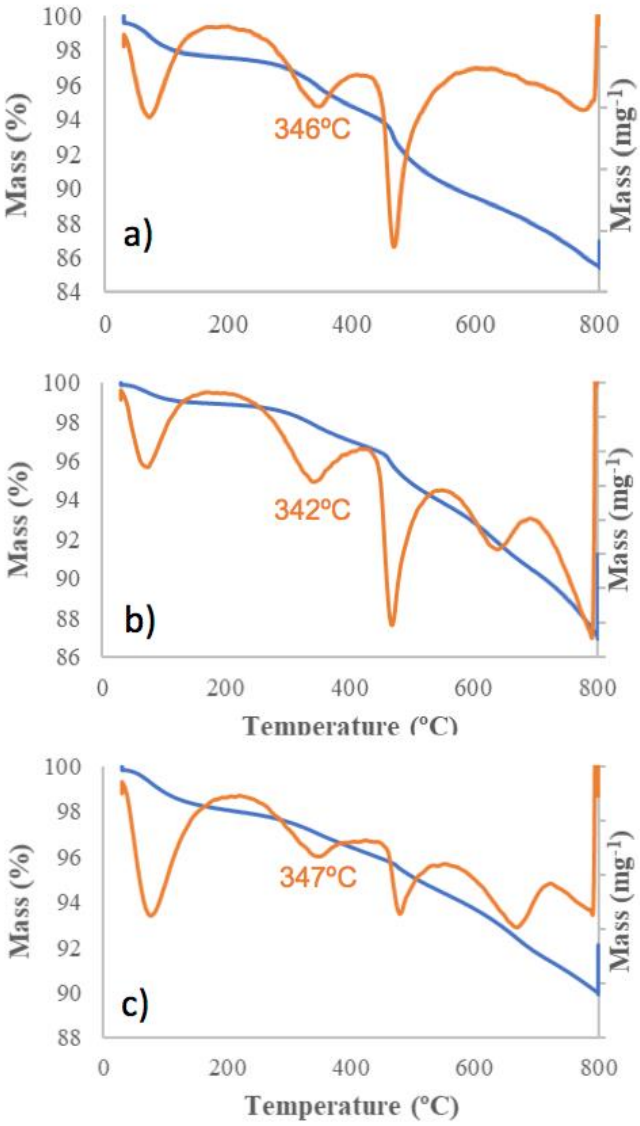

Figure 4

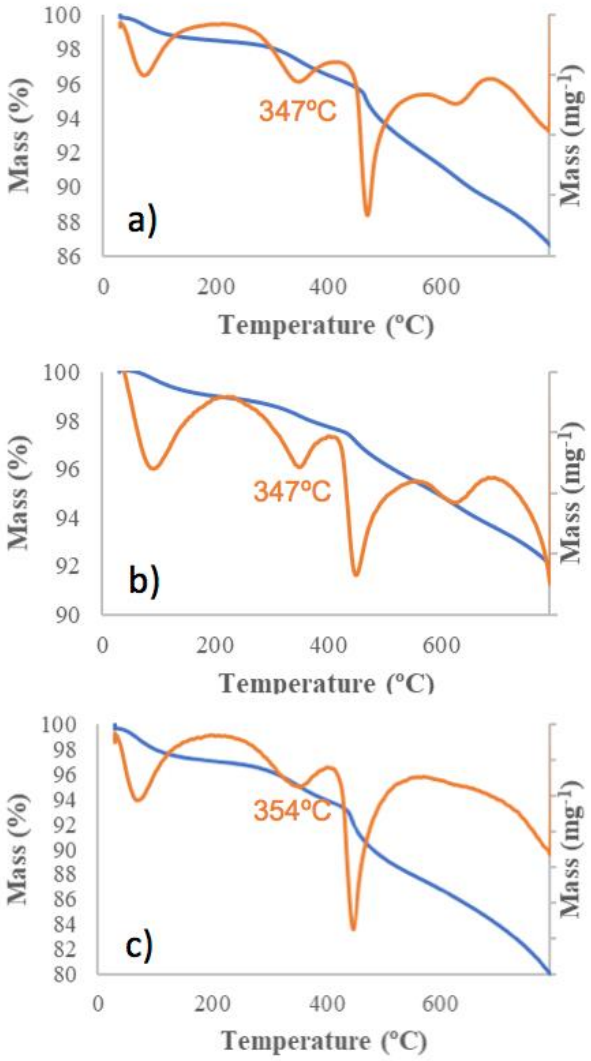
100
98
96
94
92
90
88
86
Mass (%)
347°C
a)
0
200
400
600
Temperature (°C)
Mass (mg-1)
100
98
96
94
92
90
Mass (%)
347°C
b)
0
200
400
600
Temperature (°C)
Mass (mg-1)
100
98
96
94
92
90
88
86
84
82
80
Mass (%)
354°C
c)
0
200
400
600
Temperature (°C)
Mass (mg-1)

Figure 5

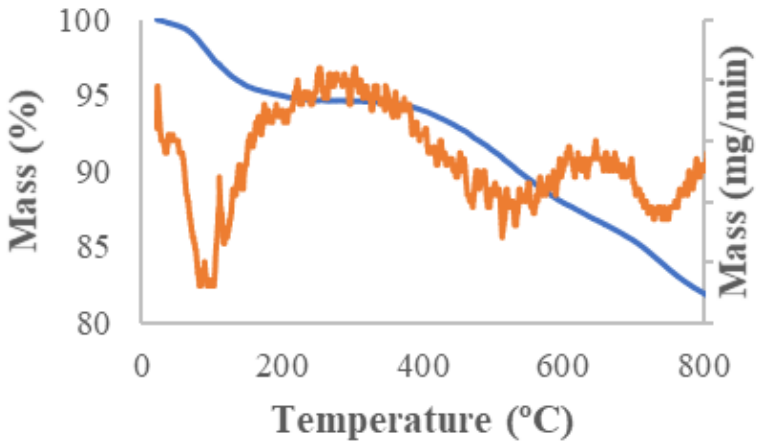

Figure 6

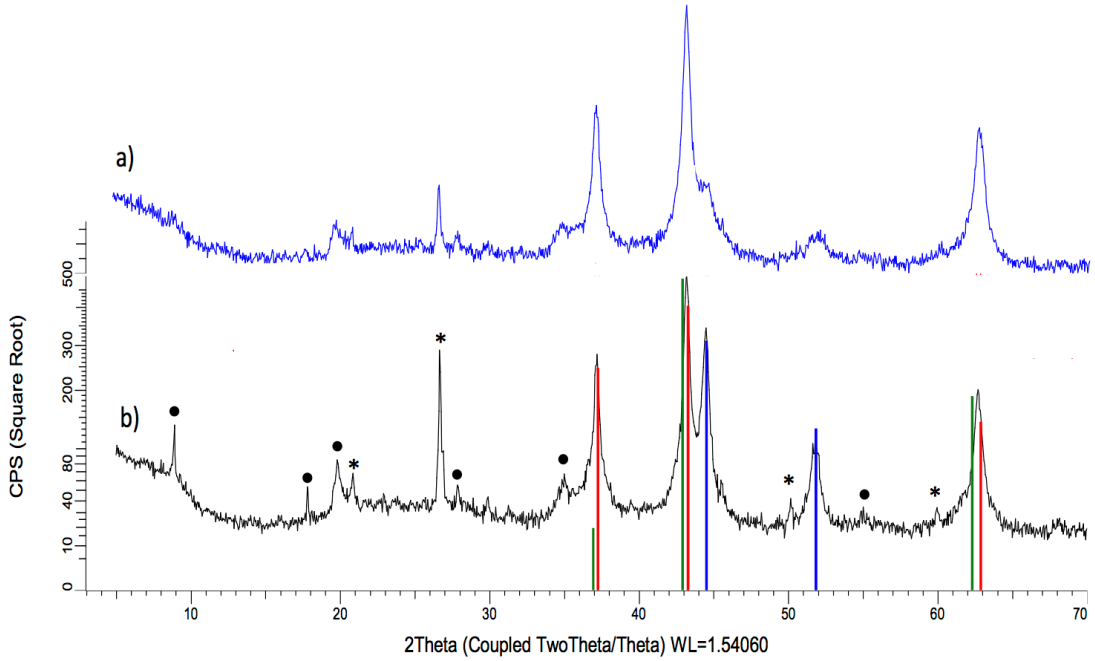
a)
b)
CPS (Square Root)
0
10
40
80
200
300
500
10
20
30
40
50
60
70
2Theta (Coupled TwoTheta/Theta) WL=1.54060

Figure 7

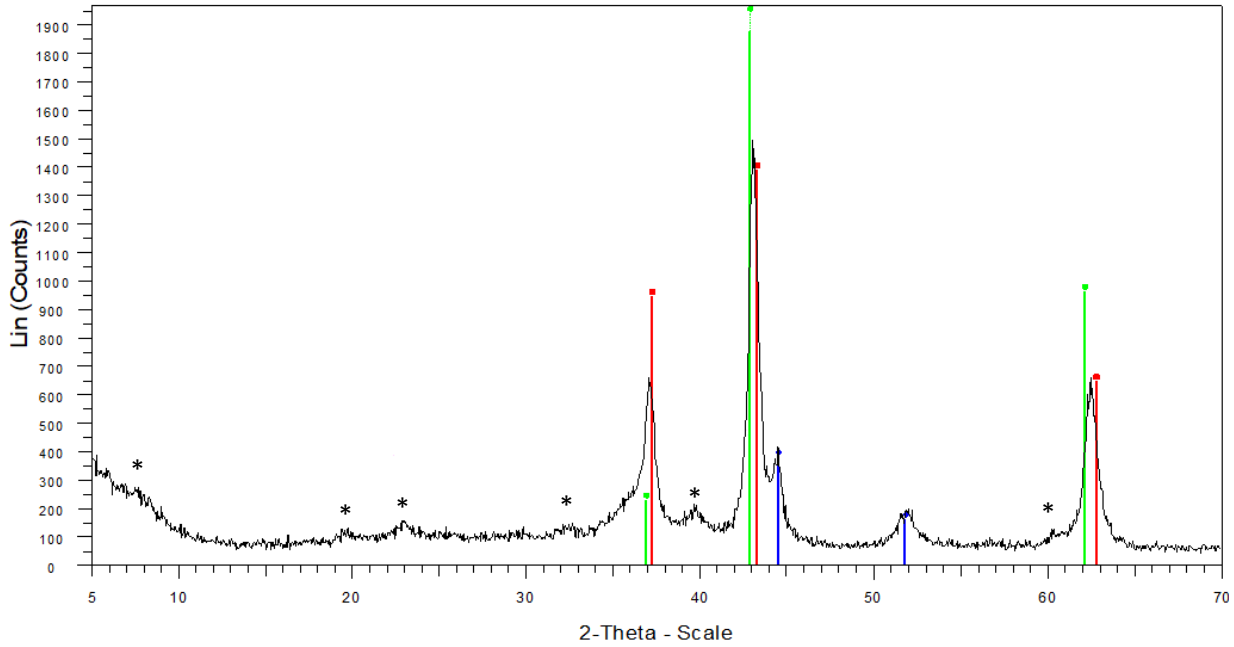
Lin (Counts)
2-Theta - Scale
0
100
200
300
400
500
600
700
800
900
1000
1100
1200
1300
1400
1500
1600
1700
1800
1900
5
10
20
30
40
50
60
70

Figure 8

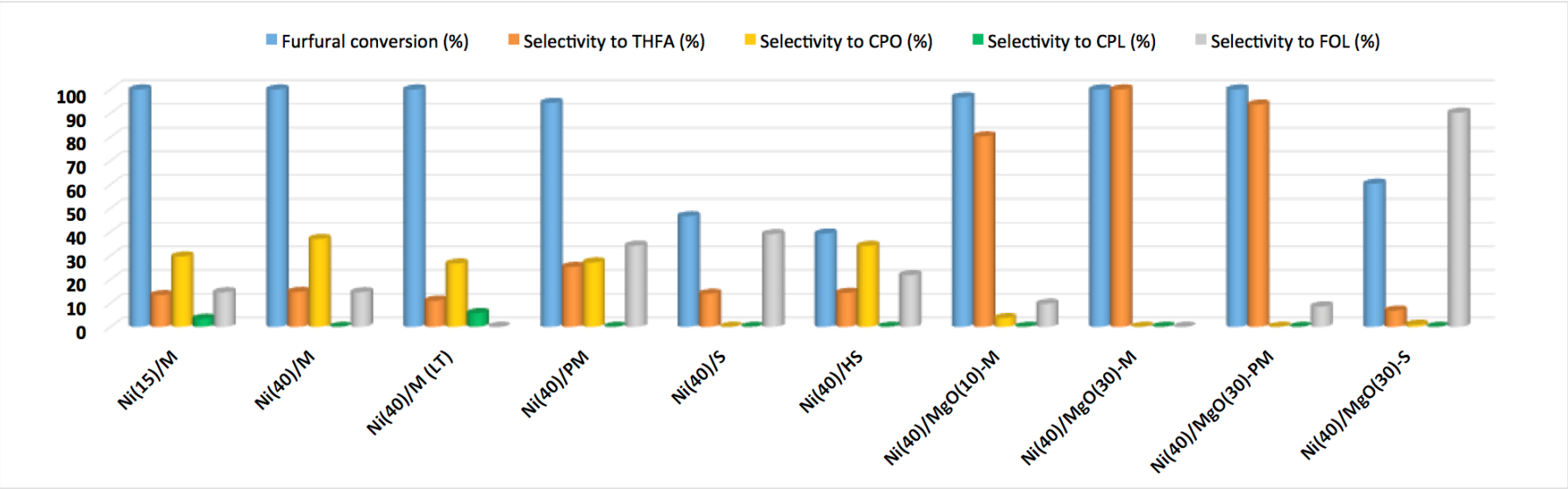
Furfural conversion (%)
Selectivity to THFA (%)
Selectivity to CPO (%)
Selectivity to CPL (%)
Selectivity to FOL (%)
100
90
80
70
60
50
40
30
20
10
0
Ni(15)/M
Ni(40)/M
Ni(40)/M (LT)
Ni(40)/PM
Ni(40)/S
Ni(40)/HS
Ni(40)/MgO(10)-M
Ni(40)/MgO(30)-M
Ni(40)/MgO(30)-PM
Ni(40)/MgO(30)-S

Figure 9

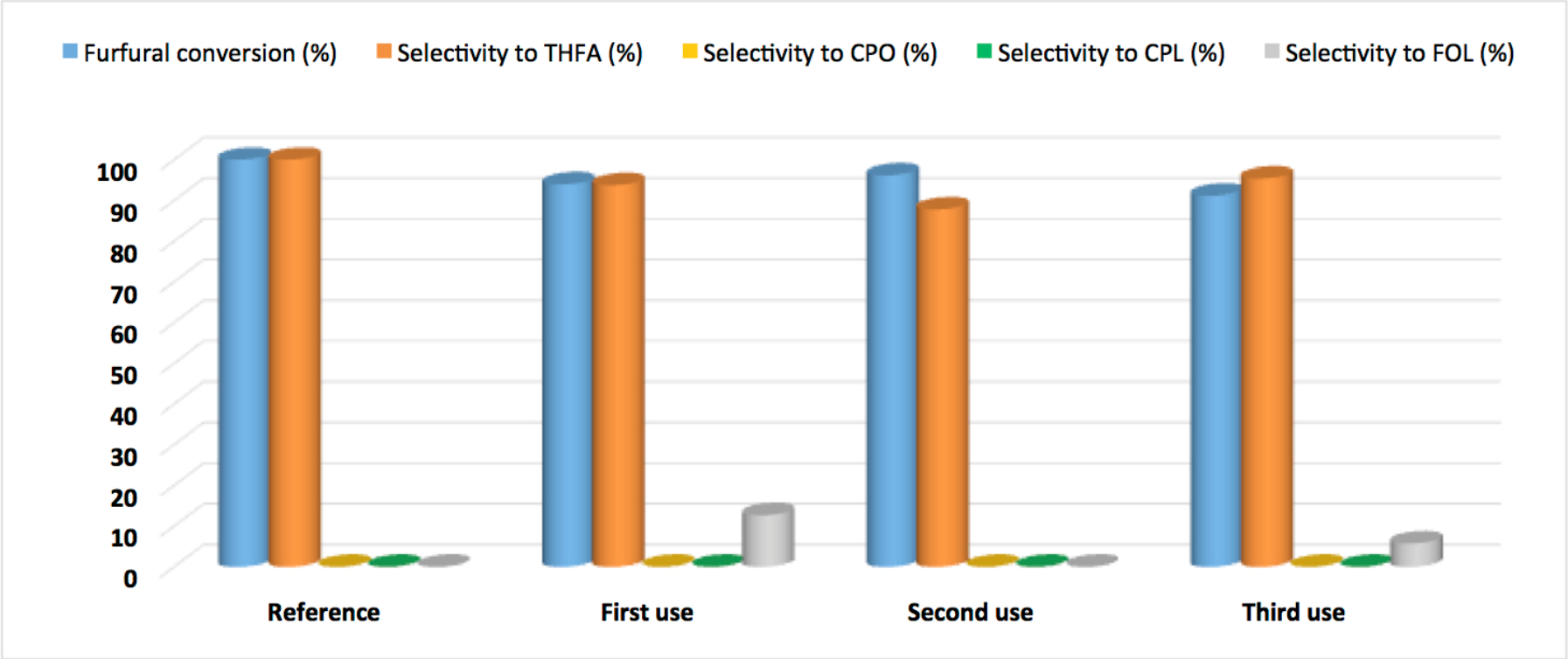
Furfural conversion (%)
Selectivity to THFA (%)
Selectivity to CPO (%)
Selectivity to CPL (%)
Selectivity to FOL (%)
100
90
80
70
60
50
40
30
20
10
0
Reference
First use
Second use
Third use

Figure 10